Non-Covalent Interactions of Uranyl Complexes: A Theoretical Study

James A. Platts[a*] and Robert J. Baker[b]

[a] School of Chemistry, Cardiff University, Park Place, Cardiff CF10 3AT, UK.

[b] School of Chemistry, University of Dublin, Trinity College, Dublin 2, Ireland.

* Author for correspondence

Email: platts@cardiff.ac.uk

Phone: +44-2920-874950

Abstract

We report a set of theoretical calculations designed to examine the potential of model uranyl complexes to participate in hydrogen- and halogen-bonding. Potential energy scans for the interaction of $[UO_2Cl_2(H_2O)_3]$ and $[UO_2(NCSe)_2(H_2O)_3]$ with a single water molecule demonstrate that uranyl is a weak hydrogen bond acceptor, but that equatorially coordinated water is a strong hydrogen bond donor. These predictions are supported by a survey of contacts reported in the Cambridge Structural Database. At the minima of each scan, we show that the interaction energy is only weakly dependent on the choice of theoretical method, with standard density functional theory methods comparing well with coupled-cluster, MP2 and double-hybrid DFT predictions. Geometry optimisation of a 1:1 uranyl:water complex results in a cyclic structure, in which vibrational frequencies, atoms-in-molecules and natural bond orbital analysis support the weakness of U—O_{yl} as acceptor. The origin of this behaviour is traced to the electronic structure of uranyl, and in particular covalency in the U—O_{yl} bonds resulting from donation into formally empty 5f and 6d orbitals on U.

Introduction

The chemistry of the uranyl ion, once dominated by its aqueous chemistry, has recently expanded into the field of supramolecular chemistry.[1] Different dimensionalities in the formation of the hybrid materials are now possible though the control given by crystal engineering. Judicious choice of equatorial ligands can give distinct and easily modifiable structures: excellent examples are shown by the use of carboxylates.[2] Simple oxalates can give dimeric species or higher nuclearity[3] species to form chains; simple monofunctionalised carboxylic acids result in monodentate and bridging modes, while larger, more complex acids can yield MOF assemblies[4] and polycatenated frameworks.[5] Further methods for forming coordination polymers invoke the tendency for the hydrated uranyl ion to hydrolyse to form, sometimes unpredictably, oxo and hydroxo bridged systems. Other structural motifs can be formed from heterobimetallic uranyl coordination polymers.[6]

Control of the geometry outside the coordinated equatorial ligands is more of a challenge for traditional coordination chemistry. Cation-cation interactions have been found to extend this dimensionality: selected examples include $[UO_2(NO_2TA)_2(H_2O)]$ (NO_2TA = 2-nitroterephthalic acid)[7] or the purely inorganic $Cs_4[(UO_2)_7(WO_5)_3O_3]$.[8] More recently the supramolecular chemists' arsenal of non-covalent interactions have featured in uranyl crystal chemistry. Hydrogen bonding between a $[UO_2Cl_4]^{2-}$ anion and bipyridinium cations afford various topologies according to the nature of the cation.[9] Pérez-Conesa et al used ab initio methods to show that binding of $[UO_2(H_2O)_5]^{2+}$ to the surface of clay materials is dominated by hydrogen bonds involving equatorial OH_2 ligands as donors to O atoms in the clay.[10] Much weaker hydrogen bonding via C—H···O_{yl}—U interactions,[11] sometimes via charge assisted hydrogen bonding,[12] have been reported and can be used to selectively separate or sense the uranyl ion selectively from complex mixtures.[13] Surbella et al show how NCS^- ligands bound to uranyl lead to a wide range of non-covalent interactions, including hydrogen bonds, S···S and S···O_{yl} interactions,[14] as well as S…H-OH hydrogen bonds that facilitate formation of infinite chains.[15] Carter et al demonstrated that uranyl oxygens' participation in halogen bonding interactions with iodine determines the 3D crystal structure and spectroscopy in a range of complexes.[16] Recently, we showed that equatorial NCS^- and $NCSe^-$ ligands give rise to a range of non-covalent interactions in the solid state, including chalcogenide…chalcogenide, U—O_{yl}…H—C and S(e)…H—C hydrogen bonding.[17]

Following literature reports, including some from our groups, of the use of uranyl in supra-molecular chemistry and molecular recognition, this work concentrates on the ability of uranyl

species to engage in non-covalent interactions, and in particular hydrogen- and halogen-bonding. In this work, we use *ab initio* and density functional theory (DFT) methods to explore potential energy surfaces for hydrogen and halogen bonding of model compounds, and to benchmark the performance of different theoretical methods in calculating geometry and energy of such interactions. To avoid complications in calculating and analysing data, we selected neutral model systems with no unpaired electrons, and hence minimal spin-orbit coupling: namely $[UO_2Cl_2(H_2O)_3]$ and $[UO_2(NCSe)_2(H_2O)_3]$. Theoretical investigation of the actinides is well developed, but the choice of methodologies is important as erroneous results can stem from certain combinations of method and basis set. The suitability of DFT for ground and excited state properties of uranium compounds was recently demonstrated through careful benchmarking:[18] our goal here is to provide a similar level of checking for non-covalent interactions.

Methods

Potential energy surfaces were calculated using the ORCA package[19], using the small core ECP60MWB 60-electron ECP/basis set on U,[20] and the def2-TZVP(-f) basis set on all remaining atoms.[21] Using this basis set, counterpoise corrected binding energies were calculated using DFT (BP86-D3,[22,23] B3LYP-D3,[24] wB97X-D3,[25] M06-2X[26] and double-hybrid B2PLYP[27]) as well as *ab initio* (HF, MP2[28] and DLPNO-CCSD(T)).[29] Further calculations used the 78-electron Lanl2DZ basis set/ECP on U,[30] and/or the 6-31G(d,p) basis set on light atoms.[31] Electronic properties were calculated using Gaussian09 at the M06-2X level with a basis set consisting of SARC-DKH all electron basis on U[32] with def2-TZVP on all remaining atoms, with relativistic effects described using the Douglas-Kroll-Hess approach.[33] Atoms-in-Molecules analysis of the resulting all-electron densities used the AIMAll package,[34] while NBO analysis was performed with NBO v3.0 within Gaussian09.[35]

Results and Discussion

Figure 1 shows the surface electrostatic potential of the two model compounds used: in both cases, relatively weak areas of negative potential ($V_S \cong$ -0.03 au) are present in the region of O_{yl}, along with deeper minima on equatorial ligands. In addition, equatorially coordinated water ligands show strong maxima ($V_S \cong$ +0.11 au) close to H. No evidence for σ-hole on Cl is observed, but this is more evident on Se ($V_S \cong$ +0.01 au). On this basis, we expect O_{yl} to act as a relatively

weak H-bond acceptor, but U-OH_2 to behave as a relatively strong donor, and Se to engage in weak halogen bonding.

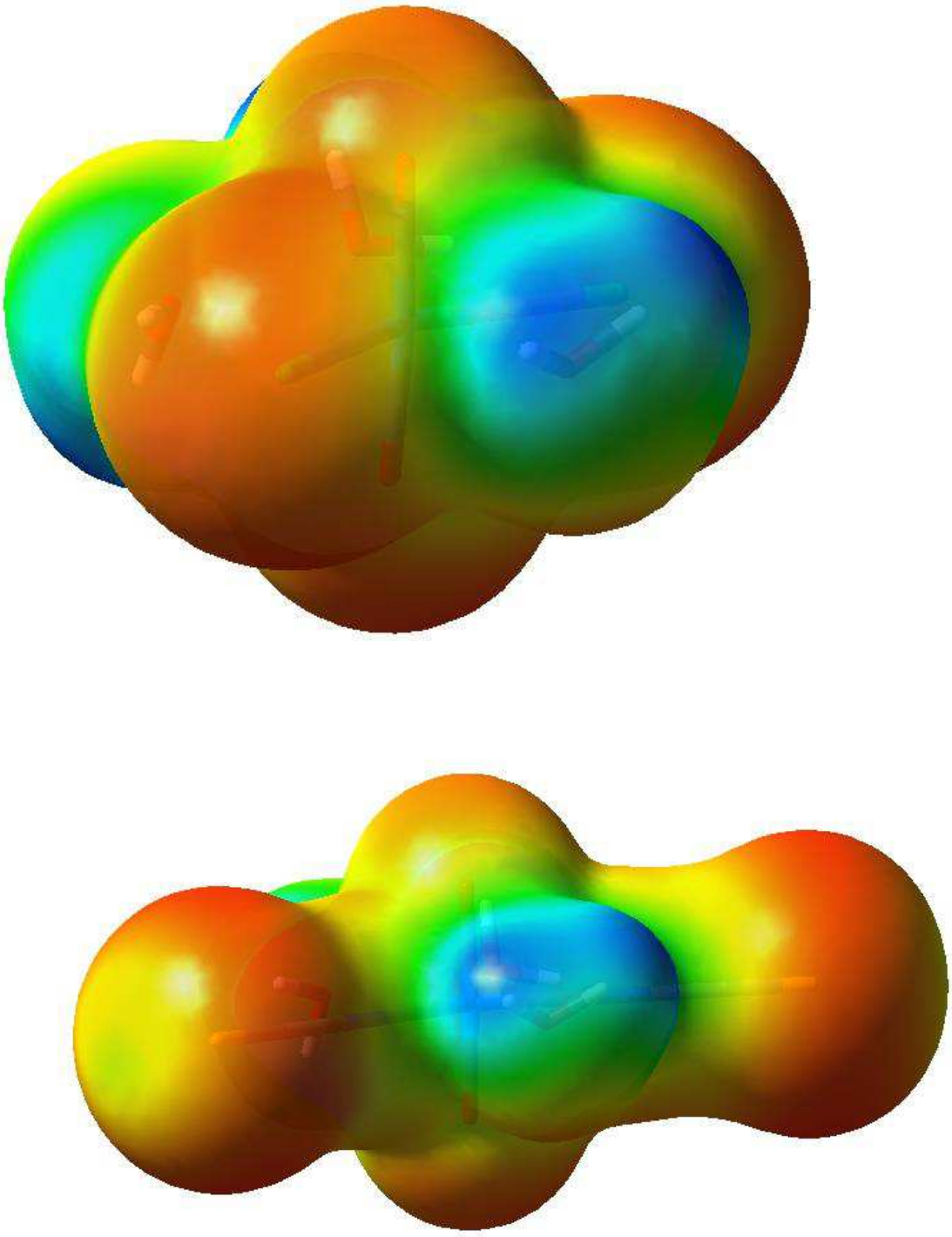

Figure 1: Electrostatic potential V_S of $[UO_2Cl_2(H_2O)_3]$ (top) and $[UO_2(NCSe)_2(H_2O)_3]$ projected onto 0.001 au isodensity surface: red = -0.04 au, blue = +0.11 au.

To quantify these expectations, a series of potential energy scans was calculated. Figure 2 shows the first of these, in which a single water molecule donates a hydrogen bond to O_{yl} directly along the U—O_{yl} vector. (This is not necessarily the optimal U—O…H angle, but our chief goal here is to assess the performance of different methods without complication of possible interactions with equatorial ligands). These data confirm the expectation of a relatively weak hydrogen bond, with maximum stabilisation of around 10 to 15 kJ mol^{-1}, depending on method, occurring close to R(O…H) = 2.10 Å. For comparison, the water dimer binding energy calculated at BP86-D3 level is -20.0 kJ mol^{-1} at R(O…H) = 1.92 Å. The predicted O…H contact is also in agreement with the crystal structure of $[UO_2Br_2(OH_2)_3]$, for which a U—O_{yl}…H distance of 2.029 Å was found.[36]

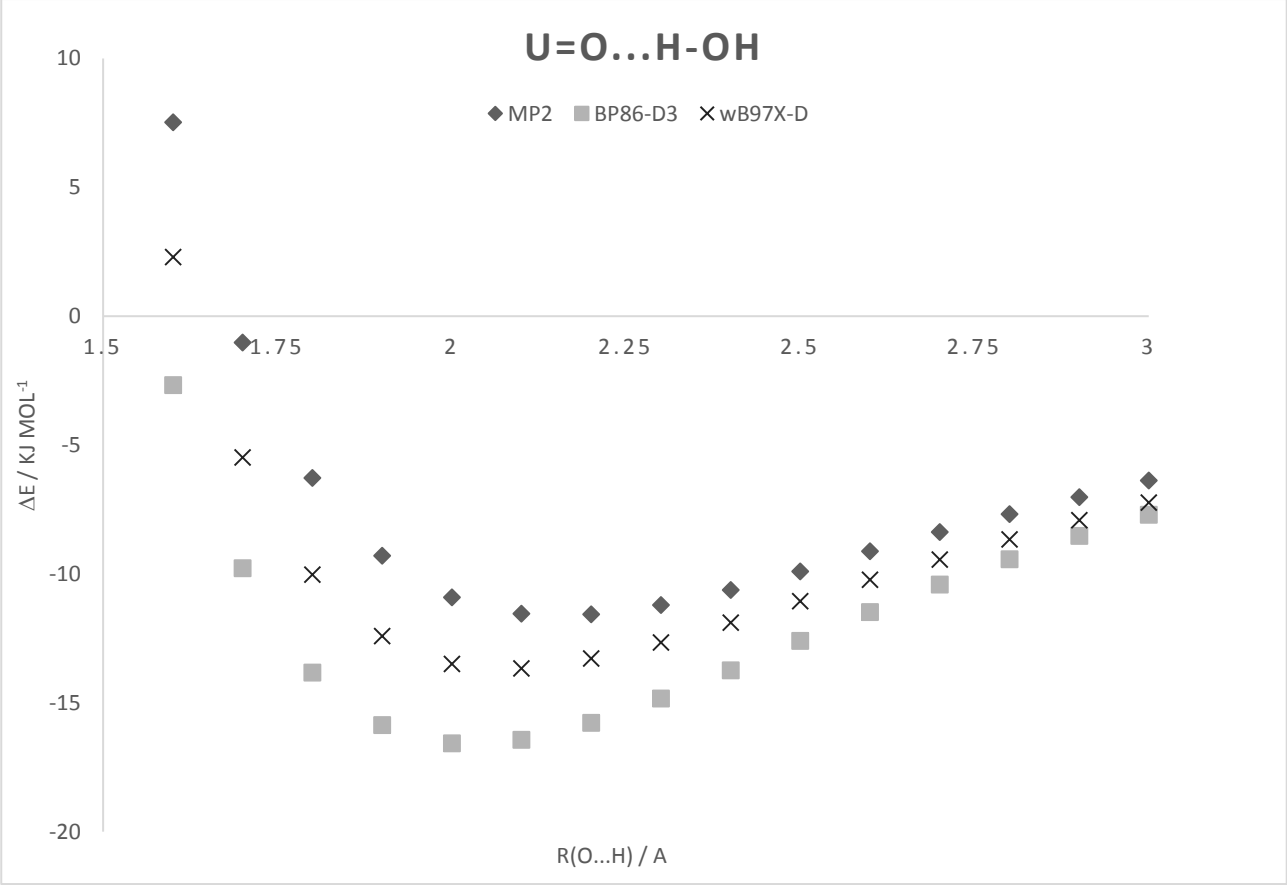

Figure 2: U—O_{yl}…H-OH Potential Energy scans for $[UO_2Cl_2(H_2O)_3]$ (at U—O…H = 180°)

Table 1: Counterpoise corrected binding energy at R(O…H) = 2.10 Å / kJ mol^{-1}

CCSD(T)	MP2	HF	BP86-D3	PBE-D3	B3LYP-D3	wB97x-D3	M06-2X	B2PLYP
-11.14	-11.55	-9.24	-15.79	-16.81	-16.44	-13.67	-12.61	-11.94

In order to further probe the strength of the H-bond, and also to better test the suitability of different methods, binding energy at R(O…H) = 2.10 Å was calculated with more methods, as reported in Table 1. All methods indicate the weakness of this hydrogen bond, between 50-75% of the binding energy of a water dimer. Taking DLPNO-CCSD(T) as a benchmark, it is evident that MP2 best reproduces this, with double-hybrid B2PLYP and meta-hybrid M06-2X also close. More conventional DFT methods with dispersion correction overestimate binding somewhat, with wB97x-D3 slightly better than BP86-D3, which in turn is rather better than B3LYP-D3. PBE-D3, which was recommended for geometries of uranium complexes,[18] performs similarly to other conventional DFT methods. It is also apparent that correlation effects are small here, since the HF binding energy is within 2 kJ mol^{-1} of the CCSD(T) one.

A further scan of the angular dependence of binding energy on U—O_{yl}…H angle is shown in Figure 3, which reveals the optimal angle to lie around 125° before rising steeply at smaller angles, and a slight (*ca.* 1 to 2.5 kJ mol^{-1}) increase in binding between 180 and 120°. Here, DFT methods result in sharper differences between 120 and 180° than does MP2, although all methods agree on the general trend.

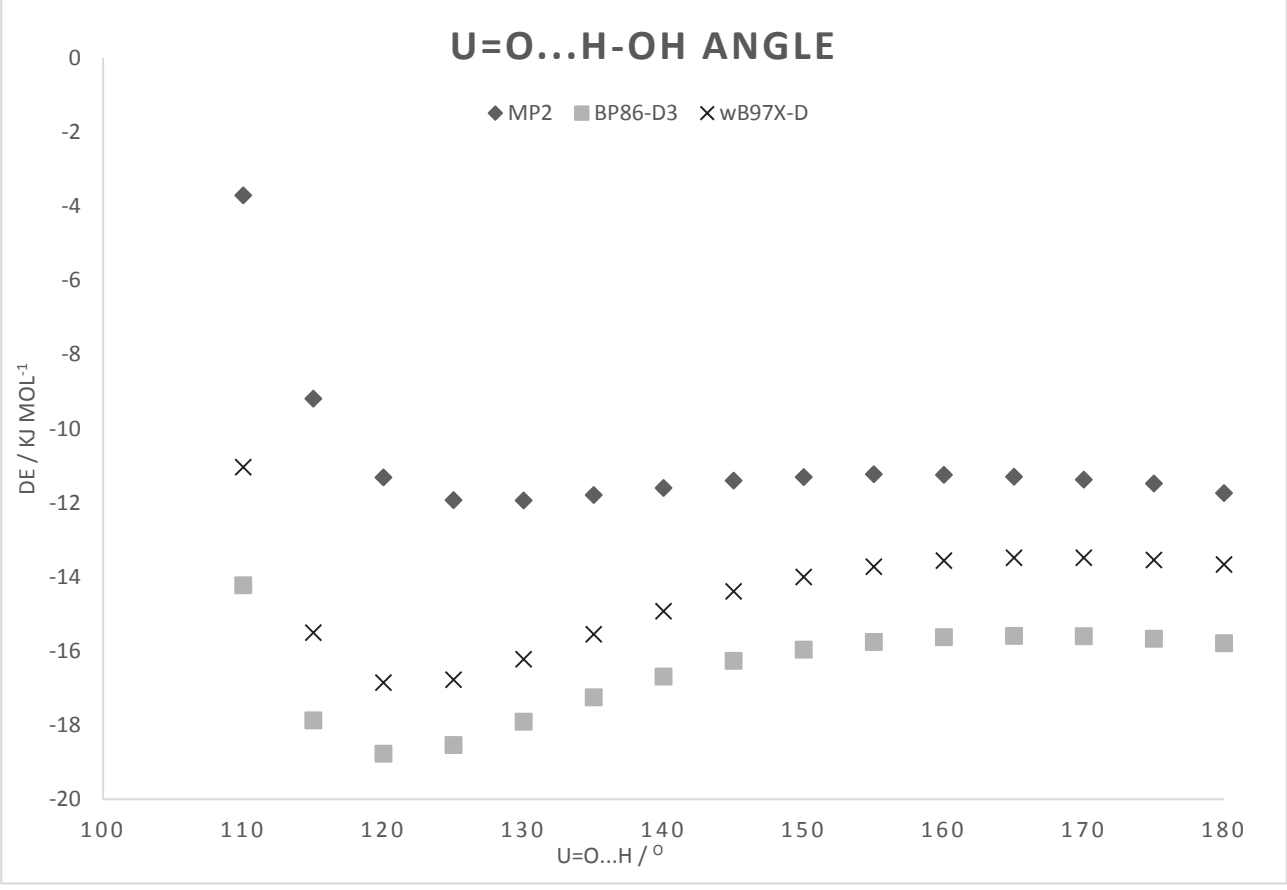

Figure 3: Potential energy scan of U—O_{yl}…H angle for $[UO_2Cl_2(H_2O)_3]$ (at R(O…H) = 2.1 Å)

A survey of the Cambridge Structural Database for U—O_{yl}…HOH contacts revealed 335 hits and a bimodal distribution with two average bond lengths at 2.06 and 2.61 Å (Figure 4). The former value is in excellent agreement with our theoretical predictions for the length of this hydrogen bond. Closer examination of Figure 4 shows a significant number of O…H contacts at 1.80 Å or even shorter. At this separation, Figure 1 shows that stabilisation is still significant, at between 5 and 10 kJ mol^{-1}: no contacts are observed at separations shorter than those for which we predict no stabilisation. The second maximum stems from further non covalent interactions, such as in the three-dimensional $[N_2C_6H_{14}]_2[(UO_2)_6(H_2O)_2F_2(PO_4)_2(HPO_4)_4]\cdot 4H_2O$, where the donor water molecule is also engaged in hydrogen bonding to the coordinated phosphate which lengthens the U-O_{yl}…HOH distance (dO…H = 2.57 Å),[37] or from water molecules that are not directly in contact with O_{yl}, for example those coordinated to equatorial ligands or simply part of the crystal lattice. The distribution of U—O_{yl}…H angle is unimodal, peaking at 132.8°; again in broad agreement with theoretical predictions. There appears to be no statistical correlation between bond length and bond angle.

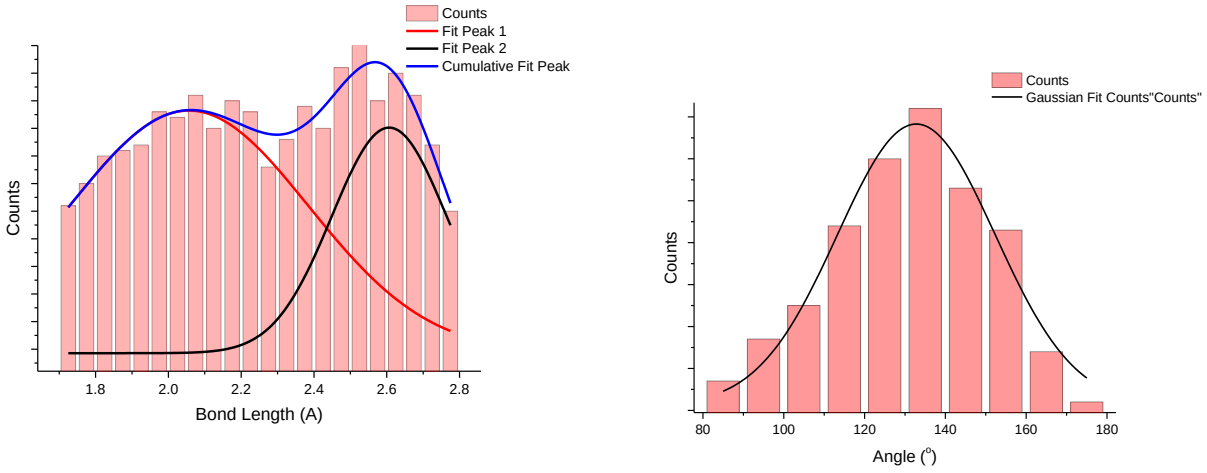

Figure 4: Results of a Cambridge Structural Database search for U—O_{yl}…HOH bond distances (left) and angles (right).

Figure 5 reports PES scans for equatorial U—O—H as donor and OH_2 as acceptor. These show that this is a rather strong H-bond, with maximum stabilisation of around -30 kJ mol^{-1} at a separation of 1.8 Å, *i.e.* shorter and stronger than in the U—O_{yl}…HOH and water dimer. At the optimal separation, binding energies with a wider variety of methods (Table 2) confirm this: the

benchmark DLPNO-CCSD(T) method indicates binding approximately 2.5 times stronger than in Table 1, and markedly stronger than in the water dimer. Again MP2 comes close to reproducing this values, and the correlation contribution to binding is small at 3.3 kJ mol^{-1}. DFT methods also work well here: double-hybrid B2PLYP is again the best of these, but here BP86-D3 actually out-performs more sophisticated methods.

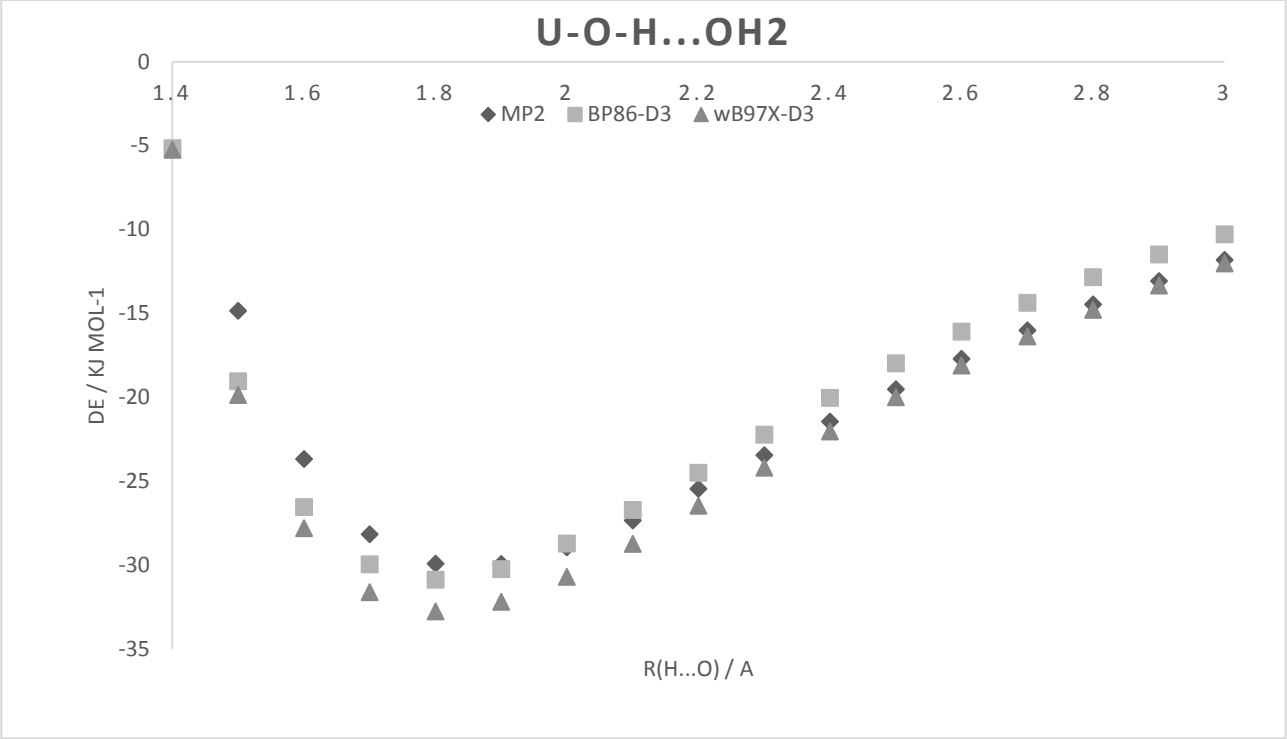

Figure 5: U-O-H…OH_2 Potential Energy scans for $[UO_2Cl_2(H_2O)_3]$ (at O…H—O = 180°)

Table 2: Counterpoise corrected binding energy at R(H…O) = 1.8 Å / kJ mol^{-1}

CCSD(T)	MP2	HF	BP86-D3	PBE-D3	B3LYP-D3	wB97x-D3	M06-2X	B2PLYP
-27.83	-29.22	-24.48	-30.88	-32.88	-33.24	-32.77	-32.62	-29.19

Full geometry optimisation using BP86-D3 was then performed, starting from the minimum of the above PES scans, without any geometrical or symmetry constraint. This results in a cyclic structure containing U=O…H-OH and U-O-H…OH_2 H-bonds, as shown in Figure 6. The former has R(O…H) = 1.931 Å, *i.e.* markedly shorter than the minimum of the PES scan but still slightly longer than the equivalent distance in the water dimer. The U—O_{yl}…H angle is 120.0°, very close to the minimum of the angular PES scan, while at O…H-O = 147.7° this H-bond is far from linear, presumably as a

result of formation of a second H-bond to equatorial water. The U—O—H…OH_2 H-bond is short, R(O…H) = 1.648 Å, and more linear than the first, O…H-O = 163.9°. Donor H-O bonds are found to be longer when H-bonded than in free water: in the U—O_{yl}…H interaction, R(O-H) = 0.987 Å (*cf.* 0.972 in H_2O), but in U-O-H…OH_2 the O-H distance of 1.015 Å represents a significant increase due to H-bonding. The counterpoise corrected binding energy of this complex is -60.10 kJ mol^{-1}, *i.e.* rather more than the sum of individual H-bond strengths found above. This is most likely due to geometrical relaxation, especially of O—H bond lengths and U—O_{yl}…H angle, which was not accounted for in rigid PES scans.

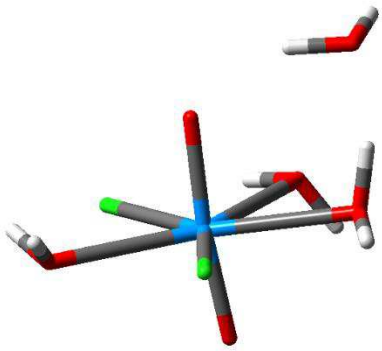

Figure 6: Optimised geometry of $[UO_2Cl_2(H_2O)_3]…H_2O$

Harmonic frequency calculation at the optimal geometry confirms this structure as a true minimum, and also reveals the effect of H-bonding on O—H and U—O_{yl} stretching modes that are often used as diagnostics of covalent and non-covalent interactions, respectively. Normal modes corresponding to O—H stretches in **O—H**…OU and U**O—H**…OH_2 are predicted to have vibrational wavenumbers of 3470 cm^{-1} and 2948 cm^{-1}, respectively, indicating substantial redshift compared to free water (3675 & 3782 cm^{-1}). Both are predicted to be strongly absorbing in infra-red. Two further normal modes, for U—O_{yl} asymmetric and symmetric stretches are predicted to lie at 913 and 816 cm^{-1} (compared to 934 and 844 cm^{-1} in the free complex). The U—O_{yl} stretch is often used as a probe of equatorial covalency:[38] our result indicate that shifts of 20 to 30 cm^{-1} can result from hydrogen bonding, which should be taken into account when such stretches are used as a proxy.

NBO analysis of the optimal geometry further highlights the relatively weak nature of H-bonds to O_{yl}: second-order perturbation analysis indicates donation from U—O_{yl} bond orbital to **H-O**H σ^* corresponding to stabilisation of 23.7 kJ mol^{-1}. By comparison, donation from water O LP to **H-O**U

σ* contributes 128.5 kJ mol^{-1} to the stability of the complex. AIM analysis (Table 3) further supports this picture: both H-bonds have properties at relevant bond critical points typical of hydrogen bonding, but by every measure the latter is markedly stronger than the former. The effect of H-bonding on the uranyl bonds is also evident: the U—O_{yl} that acts as an acceptor is notably weaker than the bond not involved in H-bonding, with ρ_{BCP} and bond order reduced by around 20%. As with U—O_{yl} stretch, such data has been used to test for covalency in equatorial coordination.[39] Our data indicate that the effects of hydrogen bonding, while relatively subtle, are of a similar order to those observed due to covalency. AIM data also reflects the stronger redshift of O—H stretch where this bond serves as the donor in the stronger hydrogen bond, with most measures of bond strength around 10% lower.

Table 3: AIM data for optimal geometry of $[UO_2Cl_2(H_2O)_3]\ldots H_2O$

	ρ	$\nabla^2\rho$	G	V	H	Bond Order
UO...H	0.021	+0.124	+0.028	-0.024	+0.004	0.031
OH...O	0.033	+0.244	+0.059	-0.057	+0.002	0.034
U—O_{yl} 1 [a]	0.292	+0.586	+0.394	-0.641	-0.247	1.782
U—O_{yl} 2 [b]	0.313	+0.612	+0.437	-0.720	-0.283	1.946
O-H…OU	0.331	-2.374	+0.011	-0.675	-0.664	0.543
O-H…OH_2	0.301	-2.130	+0.035	-0.602	-0.567	0.451

[a] H-bond acceptor; [b] not H-bond acceptor

Figure 7 shows potential energy scans for halogen bonding in $[UO_2(NCSe)_2(H_2O)_3]\ldots H_2O$, revealing very weak stabilisation of between 1 and 3 kJ mol^{-1} at minima corresponding to R(Se…O) ≅ 3.3 to 3.5 Å. The weakness of this binding is demonstrated by data in Table 4, where *ab initio* DLPNO-CCSD(T) and MP2 values are less than 1 kJ mol^{-1}, and Hartree-Fock is non-binding. This indicates that binding is driven by correlation effects such as dispersion, and that in this case at least there is little or no electrostatic contribution to this 'pseudo-halogen bonding'.

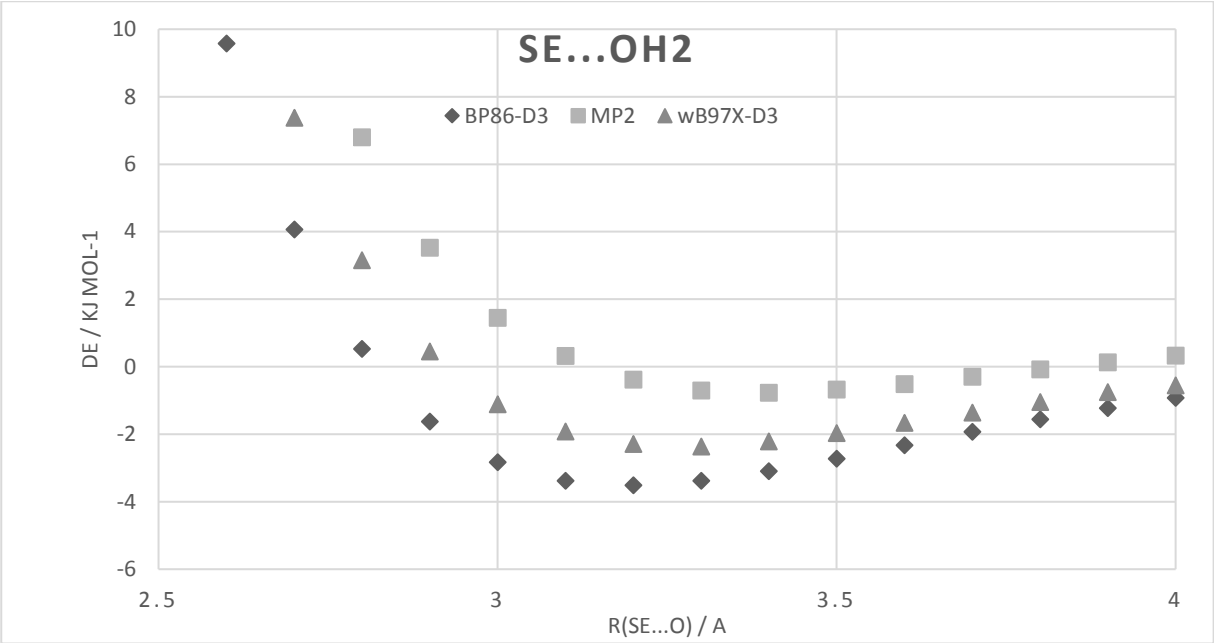

Figure 7: Potential energy scan of R(Se…O) in $[UO_2(NCSe)_2(H_2O)_3]…H_2O$

Table 4: Counterpoise corrected binding energy at R(Se…O) = 3.3 Å / kJ mol^{-1}

CCSD(T)	MP2	HF	BP86-D3	B3LYP-D3	wB97x-D3	M06-2X	B2PLYP
-0.56	-0.71	+2.23	-3.37	-3.65	-2.36	-2.75	-0.88

Recent work from Cahill's group suggested the use of halogen bonding as a means to effect supramolecular recognition of uranyl ions without the risk of hydrolysis that stems from hydrogen bonding.[16] We have therefore carried out a preliminary study of a model complex, namely $[UO_2Cl_2(H_2O)_3]…Br—Cl$, in which BrCl is a strong halogen bond donor. Figure 8 shows the optimal geometry of this complex, in which R(Br…O) = 2.521 Å and $U—O_{yl}…Br$ = 129.6°. The complex also forms an O—H…Br contact, with H…Br = 2.400 Å and 149.6°. The counterpoise corrected binding energy of this complex is -36.40 kJ mol^{-1}, *i.e.* a strong interaction albeit rather weaker than the analogous complex with H_2O.

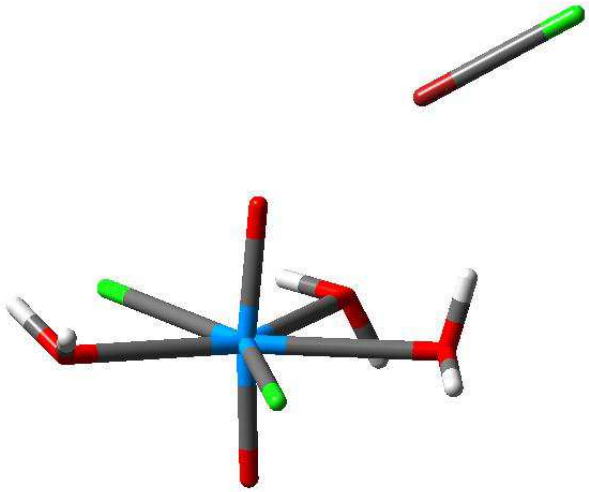

Figure 8: Optimised geometry of $[UO_2Cl_2(H_2O)_3]$…Br—Cl

All calculations reported thus far employed the small-core (60 electron) Stuttgart ECP/basis on U, previously shown to be necessary for proper description of the electronic structure of uranyl species, with triple-ζ basis on remaining atoms, widely reported as effective for DFT calculations on non-covalent interactions. However, this basis would impose significant computational overhead for larger systems than the models discussed here. It is therefore of interest to examine the performance of smaller basis sets, including larger (78 electron) core on U as well as smaller valence basis sets on light atoms. Such combinations are common for DFT calculations on d-block chemistry, and if appropriate would allow more rapid calculation of structures and binding energies, especially when combined with the computationally efficient RI-BP86-D3 method. Table 5 indicates that the predicted geometry and O—H stretches vary with choice of basis set and ECP, but within a relatively small range. U—O_{yl} and U—O_{OH2} bond lengths vary by no more than 0.03 Å, as does the length of the stronger UO—H…O H-bond. The weaker U—O_{yl}…HOH H-bond varies more with basis set: all large core ECPs predict a longer contact, highlighting the importance of explicitly including formally "core" orbitals on U in the DFT calculation for correct description of the electronic structure of uranyl. The combination of Lanl2DZ/6-31G(d,p) is particularly efficient, and might prove useful for rapid screening of possible non-covalent interactions in larger systems.

Table 5: Selected geometrical and vibrational of $[UO_2Cl_2(H_2O)_3]…H_2O$ resulting from BP86-D3 calculations with different combinations of basis set and ECP (Å, cm^{-1}, min)

U basis	O/Cl/H basis	U—Oyl[a]	U—O_{OH2}[a]	UO…H	=O…H	$\nu(OH)_w$[a]	$\nu(OH)_{eq}$[a]	Time
Stutt 60e	TZVP-f	1.813	2.506	1.648	1.931	3470	2948	187
Stutt 78e	TZVP-f	1.786	2.517	1.674	2.221	3315	3007	182
Lanl2DZ 78e	TZVP-f	1.809	2.548	1.674	2.251	3337	3002	142
Lanl2DZ 78e	6-31G(d,p)	1.818	2.512	1.618	2.175	3354	2894	58
Stutt 60e	6-31G(d,p)	1.808	2.484	1.612	2.044	3385	2866	110

[a] For bonds directly involved in hydrogen bonding; [b] Time in minutes required for analytical frequency calculation on a single processor.

The above results clearly show the weakness of O_{yl} as a hydrogen- or halogen-bond acceptor, but do not explain the origin of this behaviour. To examine this in more detail, we employed NPA and NBO analysis (Table 6). The former indicates much smaller atomic charges than formal U^{6+} and O^{2-}, reflecting the importance of covalent bonding within the uranyl unit and with equatorial ligands. O_{yl} is markedly less negative than O_{OH2}, reflecting the pattern seen in the electrostatic potential. Overall, the UO_2 unit is slightly (+0.08 e) positive, balanced by larger negative (-0.35 e) and positive (+0.21 e) charges on Cl and OH_2 units, respectively. The importance of covalency is also seen in electron configurations: formally empty valence orbitals on U exhibit significant population, most notably in 5f and 6d. Also, the ratio of p to s population in O_{yl} is smaller (2.72) than in O_{OH2} (3.04), but not to the extent that assignment of the former as sp^2 and the latter sp^3 seems warranted.

Table 6a: Natural population analysis of $[UO_2Cl_2(H_2O)_3]$

Atom	Charge	Config
U	+1.18	$7S^{0.23}\ 5f^{2.37}\ 6d^{1.69}\ 7p^{0.47}$
O_{yl}	-0.55	$2S^{1.76}\ 2p^{4.79}$
O_{OH2}	-0.83	$2S^{1.69}\ 2p^{5.13}$
Cl	-0.35	$3S^{1.85}\ 3p^{5.51}$
H	+0.52	$1S^{0.47}$

Table 6b: Natural bond orbital analysis of $[UO_2Cl_2(H_2O)_3]$

Bond A-B	Occ	Energy	%A	%B	Assignment
U=O	1.99	-1.341	10	90	σ_u
U=O	1.98	-0.473	20	80	π
U=O	1.98	-0.481	20	80	π
U=O	1.87	-0.557	16	84	σ_g
U-O	1.98	-0.818	8	92	
U-Cl	1.99	-0.369	5	95	

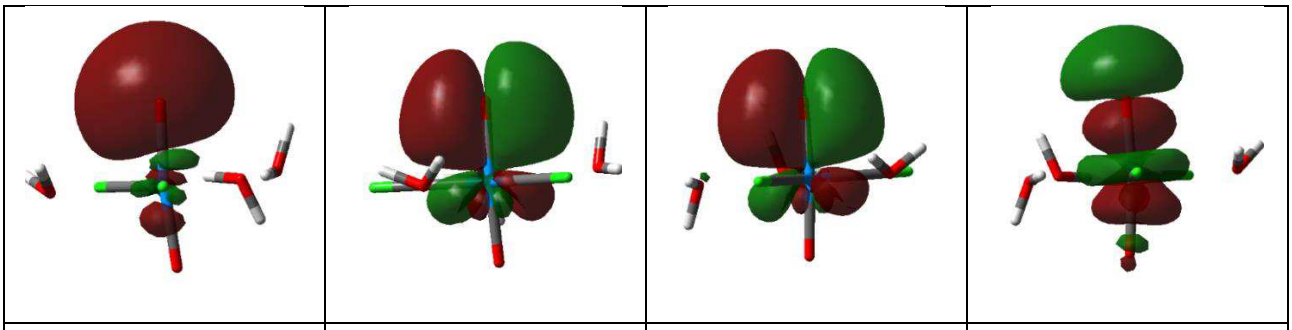

σ_u	π	π	σ_g

Figure 9: U-O "bonding" NBOs $[UO_2Cl_5(H_2O)_3]$

NBO data (Table 6b and Figure 9) sheds further light on the electronic structure of $[UO_2Cl_5(H_2O)_3]$ and its effect on H-bond acceptor ability. As set out in Kaltsoyannis's review,[40] there are 4 molecular orbitals involved in U=O bonding that transform as π_g, π_u, σ_g and σ_u in the $D_{\infty h}$ point group. The lower symmetry and involvement of equatorial ligands in this case prevents such clear cut assignments of canonical MOs, but NBOs corresponding to these are found. As shown by Fillaux et al,[41] equatorial ligands affect the energy ordering compared to that set out for bare $[UO_2]^{2+}$. Here, we find that the π-bonding NBOs are higher in energy than the σ-bonding ones, which might suggest that their chemistry should be analogous to organic or transition metal carbonyls. However, the strong overlap with 5f orbitals in both π-bonding NBOs means that these are not available as lone pairs as they would be in p- or d-block molecules. Also, the NBO that is most 'lone-pair-like' is the one denoted σ_u, but this is lowest in energy of the U—O bonding orbitals and hence less available for interaction with H-bond donors than might be anticipated from the plot alone.

Conclusions

We have used theoretical methods, supported by crystallographic data, to examine the propensity for hydrogen- and halogen-bonding within some model uranyl systems. This clearly shows the weakness of U—O_{yl} as an acceptor for hydrogen bonding: the stabilisation of a complex to water is estimated to be around -11 kJ mol^{-1}, compared to -20 kJ mol^{-1} for the water dimer using the same methods. The optimal O…H distance for this interaction is found to be around 2.10 Å, which agrees well with the most common value found in a survey of published crystal structures. In contrast, equatorially coordinated water acts as a strong H-bond donor with stabilisation in a complex with water of around -30 kJ mol^{-1}. U—O_{yl} is also found to be a viable acceptor for halogen bonding,

while equatorial $[NCSe]^-$ is a weak pseudo-halogen bond donor. In the model complexes considered here, water forms a cyclic hydrogen bonded complex when allowed to relax with no geometrical constraint. The dominance of the equatorial water ligand in determining the geometry and stabilisation of this complex is shown by NBO and AIM data. The weak acceptor ability of O_{yl} is proposed to stem from the covalent overlap in U—O_{yl} bonds: NBO analysis finds 4 bonding MOs corresponding largely to donation from O to U, along with significant population of formally empty valence orbitals on U, leading to reduced negative charge on O_{yl} and low-energy O-centred molecular orbitals that are relatively unavailable for interaction with hydrogen bond donors.

In the light of recent literature discussions on benchmarking of quantum chemistry,[42] this work falls more towards internal validation of approximate methodology against more quantitative data, rather than comparison against experiment. We take this approach mainly to avoid complications in interpretation of data: Figure 4 is a case in point, where a second maximum in O…H distance apparently stems from interaction modes other than the one of interest. Nevertheless, we report some experimental data here that support our theoretical predictions, and intend to further compare DFT predictions to experimental data in future.

Acknowledgements

JAP is grateful to Advanced Research Computing @ Cardiff (ARCCA) for provision of computing resources.

References

[1] Uranyl Bearing Hybrid Materials: Synthesis, Speciation, and Solid State Structures. M. B. Andrews, C. L. Cahill, *Chem. Rev.* 2013, **113**, 1121-1136.

[2] The crystal chemistry of uranium carboxylates. T. Loiseau, L. Mihalcea, N. Henry, C. Volkringer *Coord. Chem. Rev*. 2014, **266-267**, 69-109.

[3] Actinide oxalates, solid state structures and applications. F. Abraham, B. Arab-Chapelet, M. Rivenet and C. Tamain. *Coord. Chem. Rev*. 2014, **266-267**, 28-68.

[4] Actinide-based MOFs: a middle ground in solution and solid-state structural motifs. Ekaterina A. Dolgopolova, Allison M. Rice and Natalia B. Shustova, *Chem. Commun*., 2018, DOI: 10.1039/c7cc09780h .

[5] See for example: Exploring New Assembly Modes of Uranyl Terephthalate: Templated Syntheses and Structural Regulation of a Series of Rare 2D → 3D Polycatenated Frameworks. L. Mei, C.-Z. Wang, L.-Z. Zhu, Z.-Q. Gao, Z.-F. Chai, J. K. Gibson, W.-Q. Shi, *Inorg. Chem.* 2017, **56**, 7694-7706.

[6] Recent advances in structural studies of heterometallic uranyl-containing coordination polymers and polynuclear closed species. P. Thuéry and J. Harrowfield *Dalton Trans*., 2017, **46**, 13660-13667.

[7] Three-Dimensional Hybrid Framework Containing U_2O_{13} Dimers Connected via Cation–Cation Interactions R. C. Severance, M. D. Smith, H.-C. zur Loye, *Inorg. Chem*. 2011, **50**, 7931-7933.
[8] From Two-Dimensional Layers to Three-Dimensional Frameworks: Expanding the Structural Diversity of Uranyl Compounds by Cation–Cation Interactions, B. Xiao, H. Schlenz, J. Dellen, D. Bosbach, E. V. Suleimanov, E. V. Alekseev *Cryst. Growth Des.,* **2015**, *15*, 3775.
[9] a) Supramolecular chemistry with uranyl tetrahalide ($[UO_2X_4]^{2-}$) anions N. P. Deifel, C. L. Cahill, *Comptes Rendus Chim*. 2010, **13**, 747; b) The uranyl tetrachloride anion as a tecton in the assembly of U(VI) hybrid materials N. P. Deifel, C. L. Cahill, *CrystEngComm* 2009, **11**, 2739; c) Utilizing hydrogen bonds and halogen–halogen interactions in the design of uranyl hybrid materials, M. B. Andrews, C. L. Cahill, *Dalton Trans*. 2012, **41**, 3911-3914 .
[10] Hydration and Diffusion Mechanism of Uranyl in Montmorillonite Clay: Molecular Dynamics Using an Ab Initio Potential, S. Pérez-Conesa, J. M. Martínez, E. Sánchez Marcos *J. Phys. Chem. C*, 2017, **121**, 27437–27444.
[11] (a) Comparative IRMPD and DFT Study of Fe^{3+} and UO_2^{2+} Complexation with N-Methylacetohydroxamic Acid T. Terencio, J. Roithová, S. Brandès, Y. Rousselin, M. –J. Penouilh, M. A. Meyer, *Inorg. Chem*. 2018, **57**, 1125−1135; (b) Unusual intramolecular CH…O hydrogen bonding interaction between a sterically bulky amide and uranyl oxygen. S. Kannan, M. Kumar, B. Sadhu, M. Jaccob, M. Sundararajan, *Dalton. Trans.* **2017**, 46, 16939-16946; (c) Role of the Uranyl Oxo Group as a Hydrogen Bond Acceptor. L. A. Watson, B. P. Hay, *Inorg. Chem.* 2011, **50**, 2599-2605; (d) Oxo ligand functionalization in the uranyl ion (UO_2^{2+}). S. Fortier, T. W. Hayton, *Coord. Chem. Rev.* 2010, **254**, 197-214.
[12] Charge-Assisted Hydrogen-Bonding and Crystallization Effects within U^{VI} Glycine Compounds. J. de Groot, B. Cassell, M. Basile, T. Fetrow, T. Z. Forbes, *Eur. J. Inorg. Chem.* 2017, 1938–1946.
[13] See for example (a) A. C. Sather, O. B. Berryman, J. Rebek, Jr. Selective recognition and extraction of the uranyl ion from aqueous solutions with a recyclable chelating resin. *Chem. Sci.* 2013, **4**, 3601-3605; (b) B. F. Parker, A. S. Knight, S. Vukovic, J. Arnold, M. B. Francis, A Peptoid-Based Combinatorial and Computational Approach to Developing Ligands for Uranyl Sequestration from Seawater. *Ind. Eng. Chem. Res.* 2016, **55**, 4187−4194; (b) A. C. Sather, O. B. Berryman, J. Rebek, Jr., Selective Recognition and Extraction of the Uranyl Ion. *J. Am. Chem. Soc.* 2010, **132**, 13572–13574; (c) T. S. Franczyk, K. R. Czerwinski, K. N. Raymond, Stereognostic Coordination Chemistry. 1. The Design and Synthesis of Chelators for the Uranyl Ion. *J. Am. Chem. Soc.* 1992, **114**, 8138-8146.
[14] Thermochromic Uranyl Isothiocyanates: Influencing Charge Transfer Bands with Supramolecular Structure, R. G. Surbella III, L. C. Ducati, J. Autschbach, N. P. Deifel, C. L. Cahill *Inorg. Chem.*, 2018, **57**, 2455–2471.
[15] The exploration of supramolecular interactions stemming from the [UO2(NCS)4(H2O)]2−tecton and substituted pyridinium cations, R. G. Surbella III, C. L. Cahill *CrystEngComm*, 2014, **16**, 2352 - 2364.
[16] Harnessing uranyl oxo atoms via halogen bonding interactions in molecular uranyl materials featuring 2,5-diiodobenzoic acid and N-donor capping ligands, K. P. Carter, M. Kalaja, C. L. Cahill *Inorg. Chem. Front.*, 2017, **4**, 65-78.
[17] a) Pseudohalide tectons within the coordination sphere of the uranyl ion: An experimental and theoretical study of C-H…O, C-H…S and chalcogenide non-covalent interactions, S. Nuzzo, B. Twamley, J. A. Platts, R. J. Baker, *Inorg. Chem.* 2018, 57, 3699–3712; b) A structural and spectroscopic study of the first uranyl selenocyanate, [Et4N]3[UO2(NCSe)5], Nuzzo, S. Browne, M. P. B. Twamley, M.E.G. Lyons, R. J. Baker, *Inorganics*, 2016, **4**, 1-8.
[18] The performance of density functional theory for the description of ground and excited state properties of inorganic and organometallic uranium compounds D. Reta, F. Ortu, S. Randall, D. P.

Mills, N. F. Chilton, R.E.P. Winpenny, L. Natrajan, B. Edwards, N. Kaltsoyannis, *J. Organomet. Chem.* **857**, 58-74.
[19] The ORCA program system F. Neese, *Wiley interdisciplinary Reviews - Computational Molecular Science*, 2012, **2**, 73-78.
[20] Energy-adjusted pseudopotentials for the actinides. Parameter sets and test calculations for thorium and thorium molecules W. Kuechle, M. Dolg, H. Stoll, and H. Preuss, *J. Chem. Phys.*, 1994, **100**, 7535-42.
[21] Balanced basis sets of split valence, triple zeta valence and quadruple zeta valence quality for H to Rn: Design and assessment of accuracy F. Weigend and R. Ahlrichs, *Phys. Chem. Chem. Phys*. 2005, **7**, 3297-3305.
[22] a) Density-functional exchange-energy approximation with correct asymptotic-behavior, A. D. Becke, *Phys. Rev. A*, 1988, **38**, 3098-100; b) Density-functional approximation for the correlation energy of the inhomogeneous electron gas, J. P. Perdew, *Phys. Rev. B*, 1986, **33**, 8822-24.
[23] A consistent and accurate ab initio parameterization of density functional dispersion correction (DFT-D) for the 94 elements H-Pu, S. Grimme, J. Antony, S. Ehrlich and H. Krieg, *J. Chem. Phys*., 2010, **132**, 154104.
[24] a) Density-functional thermochemistry. III. The role of exact exchange, A. D. Becke, *J. Chem. Phys*., 1993, **98**, 5648-52.; b) Development of the Colle-Salvetti correlation-energy formula into a functional of the electron density, C. Lee, W. Yang, and R. G. Parr, *Phys. Rev. B*, 1988, **37**, 785-89.
[25] Long-range corrected hybrid density functionals with damped atom-atom dispersion corrections, J.-D. Chai, M. Head-Gordon *Phys. Chem. Chem. Phys*., 2008, **10**, 6615-20.
[26] The M06 suite of density functionals for main group thermochemistry, thermochemical kinetics, noncovalent interactions, excited states, and transition elements: two new functionals and systematic testing of four M06-class functionals and 12 other functionals, Y. Zhao and D. G. Truhlar, Theor. Chem. Acc., 2008, **120**, 215-41.
[27] Analytic derivatives for perturbatively corrected “double hybrid” density functionals: Theory, implementation, and applications, F. Neese, T. Schwabe, S. Grimme, *J. Chem. Phys.* 2007, **126**, 124115.
[28] Note on an approximation treatment for many-electron systems, C. Møller and M. S. Plesset, *Phys. Rev.*, 1934, **46**, 618-22.
[29] An efficient and near linear scaling pair natural orbital based local coupled cluster method, C. Riplinger and F. Neese, *J. Chem. Phys.*, 2013, **138**, 34106.
[30] Ab initio effective core potentials for molecular calculations – potentials for K to Au including the outermost core orbitals, P. J. Hay and W. R. Wadt, *J. Chem. Phys.*, 1985, **82**, 299-310.
[31] a) Self-Consistent Molecular Orbital Methods. 9. Extended Gaussian-type basis for molecular-orbital studies of organic molecules, R. Ditchfield, W. J. Hehre, and J. A. Pople, *J. Chem. Phys*., 1971, **54**, 724.; b) Influence of polarization functions on molecular-orbital hydrogenation energies, P. C. Hariharan, J. A. Pople, *Theor. Chem. Acc*., 1973, **28**, 213-22.
[32] All-electron scalar relativistic basis sets for the actinides, D. A. Pantazis, F. Neese, *J. Chem. Theory Comput*. 2011, **7**, 677.
[33] Douglas–Kroll–Hess Theory: a relativistic electrons-only theory for chemistry, M. Reiher, Theor. Chem. Acc. 2006, **116**, 241–252.
[34] AIMAll (Version 12.06.03), T. A. Keith, TK Gristmill Software, Overland Park KS, USA, 2012.
[35] Intermolecular interactions from a natural bond orbital, donor-acceptor viewpoint, A. E. Reed, L. A. Curtiss, F. Weinhold, *Chem. Rev.*, 1988, **88**, 899-926.
[36] Synthesis and Characterization of Heavier Dioxouranium(VI) Dihalides, *Inorg. Chem*., 2004, **43** (22), pp 7120–7126.

[37] $[N_2C_6H_{14}]_2[(UO_2)_6(H_2O)_2F_2(PO_4)_2(HPO_4)_4]\cdot 4H_2O$: A New Microporous Uranium Phosphate Fluoride, M. B. Doran, C. L. Stuart, A. J. Norquist and D. O'Hare, *Chem. Mater.* 2004, **16** , 565–566

[38] $U–O_{yl}$ Stretching Vibrations as a Quantitative Measure of the Equatorial Bond Covalency in Uranyl Complexes: A Quantum-Chemical Investigation, P. Di Pietro and Andrew Kerridge, *Inorg. Chem.*, 2016, **55**, 573–583.

[39] Assessing covalency in equatorial U–N bonds: density based measures of bonding in BTP and isoamethyrin complexes of uranyl, P. Di Pietro and A. Kerridge, *Phys.Chem.Chem.Phys*., 2016, **18**,16830.

[40] Recent developments in computational actinide chemistry, N. Kaltsoyannis, *Chem. Soc. Rev*., 2003, 32, 9–16.

[41] Investigating the electronic structure and bonding in uranyl compounds by combining NEXAFS spectroscopy and quantum chemistry, C. Fillaux, D. Guillaumont, J.-C. Berthet R. Copping, D. K. Shuh, T. Tyliszczak, C. Den Auwer, *Phys. Chem. Chem. Phys*., 2010, 12, 14253-14262.

[42] Benchmarking Quantum Chemical Methods: Are We Heading in the Right Direction? R. A. Mata and M. A. Suhm, *Angew. Chem.*, 2017, 56, 11011-11018.